International Journal of Heat and Mass Transfer 127 (2018) 761–771

Contents lists available at ScienceDirect

International Journal of Heat and Mass Transfer

journal homepage: www.elsevier.com/locate/ijhmt

Switchable heat transfer in nano Janus-interface-system

Longyan Zhang [a], Jinliang Xu [a,*], Qicheng Chen [b], Sheng Wang [a]

[a] Key Laboratory of Condition Monitoring and Control for Power Plant Equipment of Ministry of Education, North China Electric Power University, Beijing 102206, PR China
[b] School of Energy and Power Engineering, Northeast Electric Power University, Jilin 132012, PR China

ARTICLE INFO

Article history:
Received 2 February 2018
Received in revised form 13 July 2018
Accepted 15 July 2018

Keywords:
Janus interface
Wettability
Temperature jump
Viscous heating
Switchable heat transfer

ABSTRACT

Janus-interface-system is referred as liquid confined between hydrophilic and hydrophobic surfaces, nanoscale energy transfer in Janus-interface-system is not understood. Here, we investigate Poiseuille flow by non-equilibrium molecular dynamics (NEMD) using argon as the working fluid. The two solid walls hold different temperatures and wettabilities. It is found that for pure heat conduction, temperature jumps are negative on hot wall but positive on cold wall to create positive heat flow from hot wall to cold wall (called positive heat transfer). However, the convective energy transfer in Janus-interface-system always behaves positive temperature jumps on the two walls due to viscous heating. We show that, lowering hot wall wettabilities creates more significant velocity and temperature slippages on hot wall than those on cold wall to steepen liquid temperature gradients in nanochannel. We further show that heat flow sign can be switched between positive and negative, by (1) keeping super-hydrophilic hot wall but changing cold wall wettabilities, (2) keeping super-hydrophilic-hot-wall/hydrophobic-cold-wall but varying external forces applied to liquid, and (3) keeping super-hydrophilic-hot-wall/hydrophobic-cold-wall but varying hot wall temperatures. All the three cases yield non-symmetry velocity profile and more sensitive changes of temperature jumps on cold wall than those on hot wall for heat transfer switch. The transition between positive and negative heat transfer occurs at the zero temperature gradient in the channel. The findings not only enhance the understating of nanoscale energy transfer in Janus-interface-system, but also provide novel working principle for nano-devices behaving temperature sensitive nature.

1. Introduction

Water on either hydrophilic or hydrophobic surface is a nature phenomenon. The beading-up of raindrops, on raincoats or the leaves of plants are frequently observed in our daily life [1]. If the gap between two hydrophobic surfaces becomes sufficiently small, water can be spontaneously ejected [2], whereas a water film confined in symmetric hydrophilic surfaces is stable at comparable spacings [3]. Recent attention has been paid to the behavior of water confined between one hydrophobic and one hydrophilic plate (called the Janus-interface), to learn how water reacts to the competing effects of the plates. Zhang et al. [4] studied water confined between adjoining hydrophobic and hydrophilic surfaces (a Janus-interface). They noted that whereas surface energetics encourage water to dewet the hydrophobic surface, the hydrophilic surface constrains water to be present, resulting in a flickering, fluctuating complex.

Channels using different materials involve many engineering applications. For example, a micro- or nanochannel can be formed by an etched silicon substrate bonded with a glass cover, for which wettabilities are different for the two materials. Assuming a pressure driven liquid flow in a nanochannel with asymmetric solid materials (Janus-interface-system), frictions in internal liquid film and at solid/liquid interface heat up liquid and cause nonuniform temperature distribution in the liquid. A temperature gradient in liquid is related to thermophoresis or thermodiffusion, in which suspensions tend to concentrate on either high- or low-temperature side depending on the sign of their thermodiffusivity [5,6]. This phenomenon could be used for particle and biomolecule separation through micro- or nanochannel.

Flow and/or heat transfer in nanochannel cannot be predicted by continuum medium mechanics [7]. This is because when channel size is down to micron or nano scale, the surface area to volume ratio is significantly large to induce apparent interfacial effect. Two types of boundary conditions should be treated: flow boundary condition and thermal boundary condition, which are coupled with each other to make the problem more complicated. Usually, slip

* Corresponding author.
E-mail address: xjl@ncepu.edu.cn (J. Xu).

https://doi.org/10.1016/j.ijheatmasstransfer.2018.07.090
0017-9310/

length L_s characterizes the degree at which the slip flow at solid-fluid interface deviates from the non-slip flow:

$$L_s = (u_l - u_w)\Big/\left.\frac{du}{dz}\right|_w = \Delta u_w \Big/ \left.\frac{du}{dz}\right|_w \quad (1)$$

where u is the streaming velocity, Δu_w is the slip velocity at the wall, z is the coordinate perpendicular to the flow direction, the subscripts of l and w represent fluid and wall, respectively.

Numerous investigations have been performed to explore slip lengths which are dependent on solid-fluid interaction strength, shear rate and channel size [8–14]. Xu and Li [11] studied flow boundary condition over multiscale size from nano to micron or even larger. They found three types of boundary conditions (slip, non-slip and locking). Slip lengths are found to be mainly relied on solid-fluid interaction parameters, whereas channel size has almost no effect on L_s. Such finding is verified by experiments in Ulmanella and Ho [12].

Similarly, Kapitza length (L_K) characterizes the degree of temperature jump across solid-fluid interface, written as

$$L_K = (T_l - T_w)\Big/\left.\frac{dT}{dz}\right|_w = \Delta T_w \Big/ \left.\frac{dT}{dz}\right|_w \quad (2)$$

where ΔT_w is the temperature jump at the interface. The acoustic mismatch model (AMM) is a simplified theory to explain thermal resistance at solid-fluid interface, based on the continuum acoustic wave traveling in dissimilar materials [15]. AMM treats phonons as plane waves that could be transmitted or reflected at the interface. The scattering mediated acoustic mismatch model (SMAMM) was developed from AMM, including more information about microscopic principles such as phonon scattering or radiative heat transfer [16]. However, SMAMM still employed simplified assumptions of molecular structure and their interactions, which are critical in nanoscale heat transfer. Both AMM and SMAMM have limitations to deal with thermal resistance across the interface. For example, surface wettability cannot be considered in these two models. Recent progress tends to use molecular dynamics (MD) simulation for thermal boundary treatment. MD results show that wetting liquid could enhance heat transmission across the interface, thus the Kapitza length L_K is reduced [17].

Slip velocity and/or temperature jump at the interface can be influenced by many factors such as solid-fluid interaction [18–20], solid structure [21], surface geometry and temperature [22,23], driving force [24,25], shear rate [26], temperature gradient [27]. Previous studies investigated how some of these parameters influence either slip velocity or temperature jump. Slip velocities are often studied in isothermal flows by neglecting viscous heating effect, while studies of temperature jump are conducted in pure heat conduction system without considering fluid flow [17].

In summary, flow and/or heat transfer in a Janus interface system is a nature phenomenon and involves many potential applications. The mechanism is not well understood. Previous studies involving Janus-interface-system treated flow problem only [28], while the coupling problem of flow and heat transfer was dealt with in nanochannel having identical solid materials [29–31].

Here, we investigate flow and heat transfer in a nanochannel having a liquid film confined between two walls having non-identical wall wettabilities. Non-equilibrium molecular dynamics (NEMD) method was described. The solid-liquid interaction is modelled using Lennard-Jones potential including two adjustable parameters. Changing the adjustable parameters yields different wettabilities of liquid argon on the two solid walls. Velocity and temperature fields are strongly deformed and become non-symmetry in the nanochannel. The wettability difference of the two solid walls, non-dimensional force applied to each liquid atom, and hot wall temperature are examined to influence the velocity and temperature distributions. Based on temperature gradients of liquid in the nanochannel, two regimes of heat transfer are identified: positive heat transfer (heat flow from hot wall to cold wall), and negative heat transfer (heat flow from cold wall to hot wall). The modulated heat flow direction and quantity in nanochannel can be applied for nano-system development such as biology species separator in terms of the temperature sensitive nature.

2. Non-equilibrium molecular dynamics simulation (NEMD)

2.1. MD simulation domain

Fig. 1a shows the computation problem, where x, y and z refer to axial flow direction, direction perpendicular to the paper plane and height direction, respectively. Because g is applied to each liquid particle, liquid argon atoms are moving along x. We note that g is a general acceleration having a unit of m/s^2, which may deviate from g = 9.80 m/s^2. The flow can be changed by changing g. The simulation box had a size of $17.15\sigma \times 11.3\sigma \times 21.2\sigma$, corresponding to 5.83 × 3.85 × 7.22 nm^3, where σ is the length scale of argon atom. The distance between the two walls is $H = 16\sigma$ = 5.41 nm. Inside the nanochannel, there are 2340 argon atoms (at its saturated liquid density). The initial liquid density ρ and temperature T are 1310 kg/m^3 and 100 K. The saturation liquid of argon is verified by the relationship between pressure and temperature. At the initial condition of 100 K, the pressure is 0.3277 MPa for argon, coming from the NIST software, respectively. The lattice parameter of liquid argon is determined based on its density and FCC structure, which is 1.72σ here.

We note that, liquid atoms are confined between the two solid walls. The number of liquid atoms is not changed during computation. The simulation system is a single-phase liquid system without phase change. Physical properties of liquids are mainly dependent on temperatures, weakly dependent on pressures. Liquid pressures have neglectable effect on flow and heat transfer. We also note that, different wall wettabilities yield different peak liquid densities near the wall. The peak density layer is very narrow in the channel height direction. The near-wall liquid compressibility would not change the bulk liquid densities. For a system having dense solid atoms, liquid atoms cannot penetrate solid wall. Thus, the interfacial parameters are not influenced by pressures. Pham et al. [32] studied the pressure effect on thermal boundary conditions, showing that Kapitza lengths are not changed versus pressures for a system with dense gold atoms. Feng and Liang [33] noted the neglectable effect of pressures on thermal boundary conditions for asymmetrical solid-liquid systems. Thus, it is not necessary to consider the pressure effect in this study.

The computation domain consists of a top wall and a bottom wall. Each wall includes eight layers of solid atoms. At initial computation stage, all solid atoms are arranged as a FCC lattice structure. There are 2688 platinum atoms for each solid wall corresponding to a density of 21.45 × 10^3 kg/m^3. For each wall, solid atoms of the four layers attaching liquid film are oscillating freely. These solid atoms deviate from initial location and exchange energy with liquid atoms. Beyond the inner four layers of solid atoms, there are two layers of solid atoms acting as the thermostat atoms to keep specific wall temperature. The outmost two layers of solid atoms are stationary, which ensures the stationary of the solid wall, from macroscopic point of view. The outer four layers, including thermostat atoms and stationary atoms are called ghost atoms. The thermostat technique is implemented using following equation [34]:

$$\frac{dp_i}{dt} = -\xi p_i + f(t) + F(t) \quad (3)$$

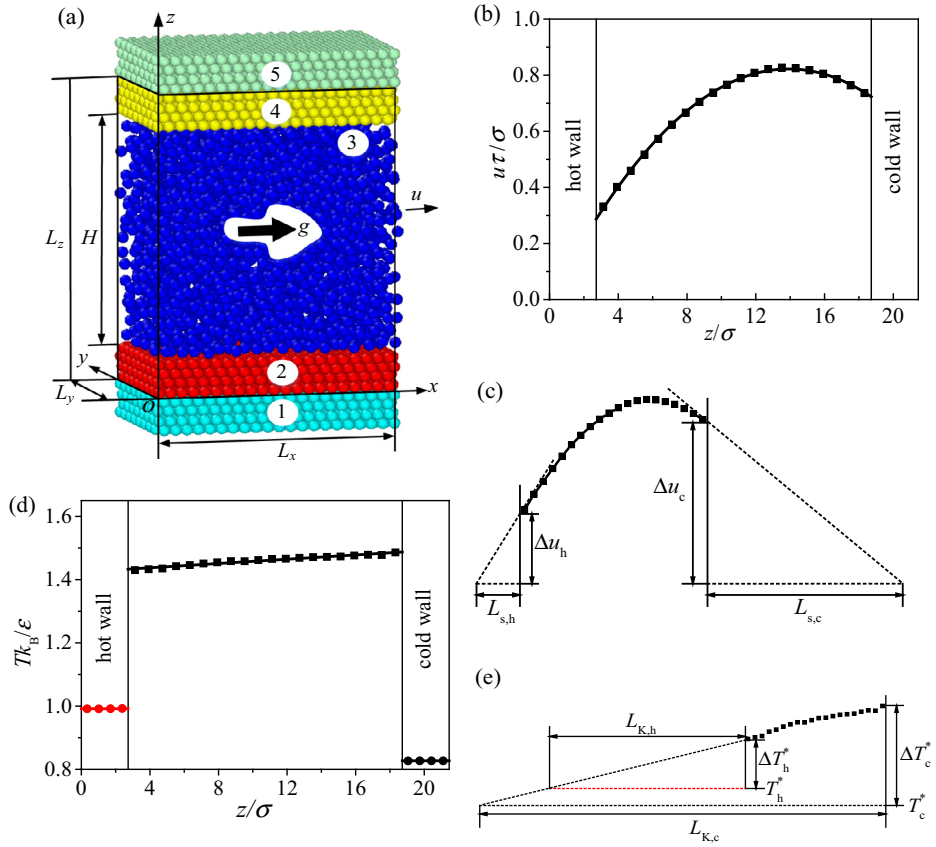

Fig. 1. The studied problem (for a, 1 and 5 are ghost atoms, 2 and 4 are wall atoms, 3 is liquid atoms; b: streaming velocities in nanochannel; c: slip velocities and lengths on two solid walls; d: temperatures in nanochannel; e: temperature jump and Kapitza lengths on interfaces. Case study for $F_g^* = 0.02$, hot wall with $T_h^* = 0.992$, $\alpha = 0.14$, $\beta = 1$; and cold wall with $T_c^* = 0.827$, $\alpha = 0.14$, $\beta = 0.5$).

where p_i is the momentum vector of solid atom i, $\xi = 168.3\tau^{-1}$ is the damping constant, $f(t)$ is the interaction force between atoms, $F(t)$ is the exciting force vector, which is randomly sampled from Gaussian distribution with zero mean average value and standard deviation of $\sigma_G = \sqrt{2\xi k_B T_w/\delta t}$, $k_B = 1.38 \times 10^{-23}$ J K^{-1} is the Boltzmann constant and $\delta t = 0.0023\tau$ is the time step.

2.2. The Lennard-Jones potential

For each liquid atom, the Newton equation is written as

$$m\frac{d\vec{r}^2}{dt^2} = \sum_{j\neq i,j=1}^{N} \vec{F}_{ij} + \sum_{j_w\neq i,j=1}^{N_w} \vec{F}_{ij_w} + mg\vec{i} \tag{4}$$

The first and second terms of right side of Eq. (4) represent the force between liquid atoms, and between liquid atom and solid atom, respectively, where m is the argon atom mass, r is the distance between liquid atom i and liquid atom j or solid atom j_w, N and N_w are the total number of liquid atoms and solid atoms, respectively, $\vec{i}$ is the unit vector along the axial flow direction. The relationship between force and potential is

$$F_{ij} = -\frac{\partial \phi_{ij}}{\partial r_{ij}} \tag{5}$$

The Lennard-Jones (L-J) potential function is used for interaction between atoms:

$$\phi(r) = 4\alpha\varepsilon\left[\left(\frac{\sigma}{r}\right)^{12} - \beta\left(\frac{\sigma}{r}\right)^{6}\right] \tag{6}$$

where ε is the energy scale, σ is the length scale, α is the potential energy factor indicating the strength of hydrophilic interaction and β is the potential energy factor indicating the attraction for hydrophobic interaction. Eq. (6) comes from Nagayama and Cheng [9]. Even though Eq. (6) uses both α and β to characterize the wettability degree between solid and liquid, we only change β to change the wettability degree but keep $\alpha = 0.14$ in this paper. For a pair of identical type atoms such as solid-solid and liquid-liquid, the parameters are set as $\alpha = 1$, $\beta = 1$. The parameters are $\varepsilon_l = 1.67 \cdot 10^{-21}$ J/K, and $\sigma_l = 3.405 \cdot 10^{-10}$ m for argon. For solid-solid interaction, the parameters are $\varepsilon_w = 8.35 \times 10^{-20}$ J/K and $\sigma_w = 2.475 \times 10^{-10}$ m.

The LJ potential parameters between a liquid atom and a solid atom come from Ref. [9]. The wall wettability can be controlled by changing β only. The platinum wall is hydrophilic with respect to argon liquid to have a contact angle of 0° by using $\alpha = 0.14$ and $\beta = 1.0$. In this paper, α is set as 0.14, β may be different for top wall and bottom wall, representing different wettabilities of the two walls (see Fig. 1a), where $\varepsilon = \varepsilon_{sl} = \sqrt{\varepsilon_l \cdot \varepsilon_w}$ and $\sigma = \sigma_{sl} = 0.5(\sigma_l + \sigma_w)$, coming from the Lorentz-Berthelot combining rule [35].

2.3. Statistical parameters

In the liquid domain, 32 bins are segmented in the z direction. Velocity along the x direction (u), density (ρ) and temperature (T) are time-averaged in each bin. Due to solid-liquid interaction, the external force applied to liquid can be transmitted to walls. To prevent walls from moving, solid atoms of outer two layers are fixed and of inner four layers are vibrating freely, sufficiently

accounting for the effect of surface flexibility on fluid motion. Temperature in the ith bin, T_i, is determined by peculiar velocity relative to streaming velocity of the atoms in the bin:

$$T_i = \frac{\sum_{i=1}^{N_i} m(v_i - u_i)^2}{(3N_i - \delta)k_B} \tag{7}$$

where N_i is the number of liquid atoms in the bin, v_i is the laboratory velocity and u_i is the mean axial velocity in the bin, k_B is the Boltzmann constant and δ is the number of degrees of freedom for the determination of the axial velocity, which is sufficiently small compared with N_i.

In Janus-interface-system with flow and heat transfer, heat fluxes across the two solid-liquid interfaces may be different, which are recorded as $q_{i,h}$ for hot wall and $q_{i,c}$ for cold wall, respectively. The two interfacial heat fluxes are determined based on energy balance between the kinetic energies supplied to heat source and subtracted from heat sink in a given period of time, which is as follows [36]

$$\Delta E = \sum_{\text{transfer}} \frac{m}{2}\left(\sum_N v_{\text{new}}^2 - \sum_N v_{\text{old}}^2\right) \tag{8}$$

where m is the mass of solid wall atoms, the subscripts "new" and "old" represent current time period and previous time period, respectively. The elapsed time during 2.0 million timestep is recorded as τ_{ela}. The heat flux through the interface q_i is

$$q_i = \frac{\Delta E}{\tau_{ela} A_{xy}} \tag{9}$$

where A_{xy} is the planar area of the computation domain. The heat flux of liquid confined in nanochannel, q, is [37]

$$q = \frac{1}{\Omega}\left[\sum_{i=1}^{N}\left(v_i' e_i + \frac{1}{2}\sum_{j=1, j\neq i}^{N} r_{ij}(F_{ij}\cdot v_i')\right)\right] \tag{10}$$

where Ω is the liquid computation domain volume, v_i' and e_i are the thermal velocity and total inner energy of atom i, the latter includes thermal kinetic energy $\frac{1}{2}mv_i'^2$ and potential energy ϕ, F_{ij} is the force acting on atom i from atom j.

In order to present results in a general sense, computations are performed using a set of non-dimensional parameters, which are expressed in Table 1. All the parameters are scaled by m, σ and ε for liquid atoms, where τ is the time scale for argon atom: $\tau = \sqrt{m\sigma^2/\varepsilon} = 2.16 \times 10^{-12}$s. The periodic boundary conditions are applied in x and y directions. Our MD simulation successfully predicts velocity and/or temperature fields in nanochannel in which the two solid walls are identical. Simulation results agree with Ref. [10,38]. We are interested in non-identical solid wall system. Fig. 1 shows an example. Nanoflow is driven by non-dimensional force $F_g^* = 0.02$. The hot wall (bottom) is with $T_h^* = 0.992$, $\alpha = 0.14$ and $\beta = 1.0$, but the cold wall (top) is with $T_c^* = 0.827$, $\alpha = 0.14$ and $\beta = 0.5$, Fig. 1 shows non-symmetric velocity and temperature profiles in the nanochannel. Due to hydrophilic hot wall and hydrophobic cold wall, slip velocities and temperature jumps are larger on the cold wall than those on the hot wall.

Table 1
The non-dimensional parameters.

Property	Parameters
Length	$r^* = \frac{r}{\sigma}$
Time	$t^* = \frac{t}{\tau}$
Force	$F^* = \frac{F\sigma}{\varepsilon}$
Temperature	$T^* = \frac{k_B T}{\varepsilon}$
Velocity	$v^* = \frac{v\tau}{\sigma}$
Heat flux	$q^* = \frac{q\sigma^3}{\varepsilon}\sqrt{\frac{m}{\varepsilon}}$

3. Effect of α and β on surface wettability

The objective of this paper is to explore different wettabilities of the two walls on velocity and temperature distributions in the nanochannel. Before presenting these results, contact angles (CA) of liquid argon on solid walls are quantified using MD approach. Different from Section 2, the CA simulation treats a single wall and liquid argon only. The simulation box had a size of $110\sigma \times 10\sigma \times 64\sigma$. A two-dimensional droplet was considered with its final diameter larger than 10 nm, thus contact angle is less influenced by droplet sizes. The computation domain contains 6690 argon atoms and 11,566 solid atoms. The contact angle simulation is a three-dimensional computation. The periodic boundary condition is applied along the axial direction x and the direction perpendicular to the paper plane y. Thus, the droplet behaves two-dimensional characteristic. The liquid momentum along x and y directions are zero to keep the droplet in the computation domain. The truncation size and timesteps were 3.0σ and 5 fs, respectively. After the initial 2 million timesteps computation, the two-dimensional argon density distribution was averaged on the xz plane, with the grid resolution of $0.2\sigma \times 0.2\sigma$. The data sampling was repeated for each 100 timesteps. The gas-liquid interface is assumed to have the density of $0.5(\rho_l + \rho_v)$, where ρ_l and ρ_v are liquid density and vapor density, respectively. After the gas-liquid interface was finalized, CA was computed based on the droplet height h in z direction and footprint radius a on solid wall. The following equation is used:

$$CA = \begin{cases} \left|-\arcsin\left(\frac{a}{R}\right)\right| & \text{if} \quad CA < \frac{\pi}{2} \\ \pi - \arcsin\left(\frac{a}{R}\right) & \text{if} \quad CA > \frac{\pi}{2} \end{cases} \tag{11}$$

where $R = (a^2 + h^2)/(2h)$. Fig. 2 presents the simulation results, in which α is 0.14, but β is changed from case to case. Two limit cases are $\beta = 0.1$ corresponding to $CA = 180°$ (super-hydrophobic surface), and $\beta = 1.0$ corresponding to $CA = 0°$ (super-hydrophilic surface). The larger β is, the solid wall is more hydrophilic. Fig. 2g shows contact angles versus β.

4. Results and discussion

We presented simulation results for (1) pure heat conduction without liquid friction in the nanochannel; (2) coupled flow and heat transfer with changed hot wall wettabilities, and (3) coupled flow and heat transfer for the combination of super-hydrophilic hot wall and hydrophobic cold wall. By comparing item 1 and items 2–3, one examines how the liquid friction influences heat transfer in the nanochannel. Results of item 2 show that, by decreasing hot wall wettabilities, liquids are traveling faster to enhance the friction effect on the hot wall, steepening the temperature gradient in the nanochannel. Within the liquid film, heat flows from hot wall side to cold wall side (positive heat transfer). On the other hand, results of item 3 show that, heat in the liquid film can either be transferred from hot wall side to cold wall side (positive heat transfer), or be transferred from cold wall side to hot wall side (negative heat transfer). Heat flow direction in the liquid film can be switched.

4.1. Pure heat conduction in the nanochannel

Liquid in nanochannel behaves pure heat conduction if no external force is applied to liquid. The friction induced heating effect does not exist. For this problem, heat is transferred from hot wall to liquid, and from liquid to cold wall. Temperature

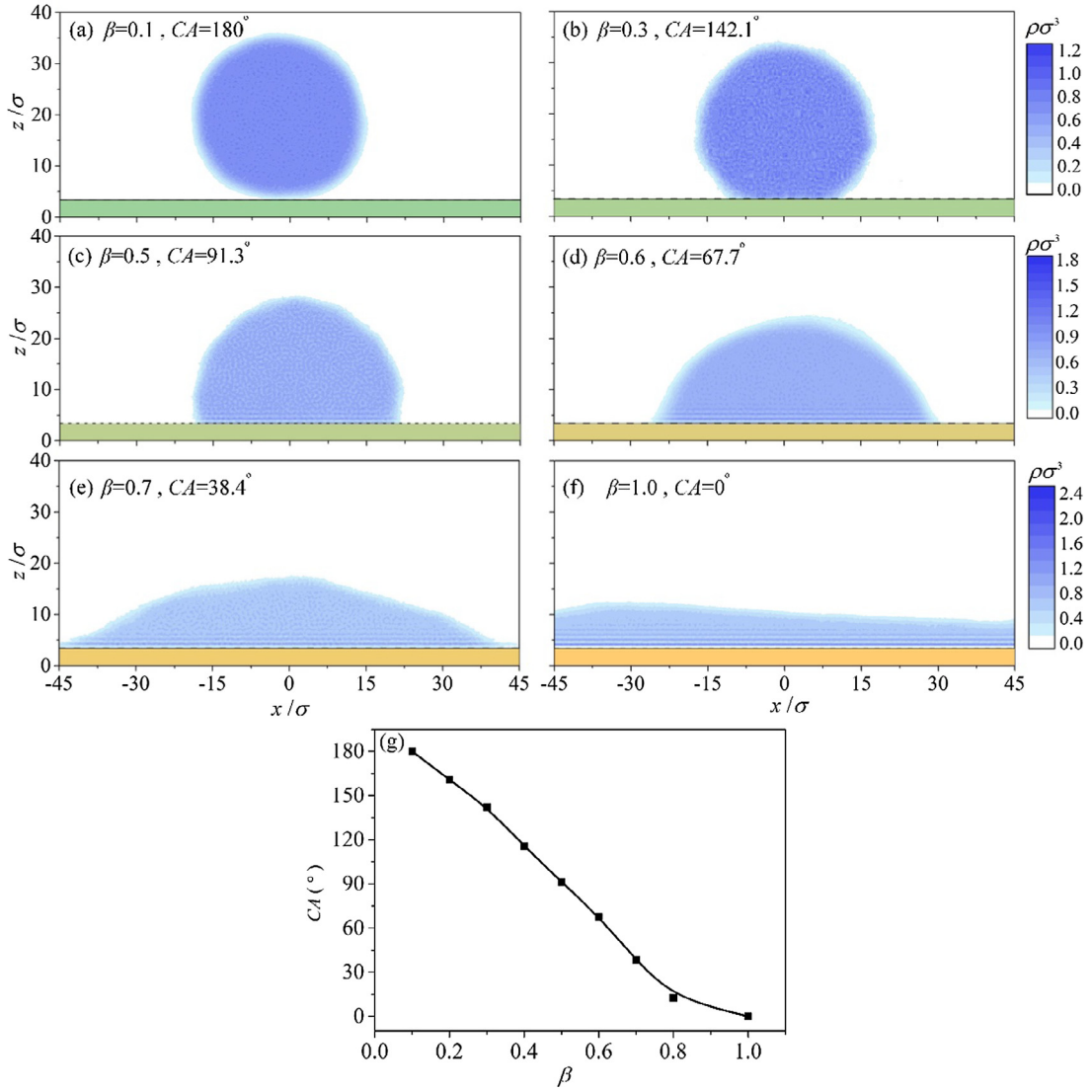

Fig. 2. Effect of β on contact angles having $\alpha = 0.14$ (a–f for droplet morphology at $\beta = 0.1$, 0.3, 0.5, 0.6, 0.7 and 1.0; g for contact angles versus β).

profiles are linear in liquid film (see Fig. 3a). It is noted that the three heat flexes $q_{i,h}$, q_l and $q_{i,c}$ are identical and share same sign. For steady heat conduction problem, because there are no heat generation and viscous heating effect in the system, the three heat fluxes should be same. We also note that there are small temperature oscillations near the two solid walls. This is due to small noise temperature signal during the MD computation and sampling process. Fig. 3b shows that the interaction between liquid atoms and solid atoms is enhanced by increasing β, which leads to a larger peak of liquid density near the cold wall. Temperature jump is negative on the hot wall, but positive at the cold wall (see Fig. 3c). Keeping super-hydrophilic hot wall (β = 1.0 and $CA = 0°$), the cold wall significantly increased non-dimensional temperature jumps ($\Delta T_c k_B/\varepsilon$) and Kapitza lengths ($L_{K,c}$), when it is changed from super-hydrophilic to hydrophobic. Fig. 3d shows that when identical wettabilities are used for the two solid walls (β = 1 and $CA = 0°$), Kapitza lengths (absolute values) nearly shrink to the same value. Heat fluxes are increased when the cold wall wettabilities are enhanced (see Fig. 3e), due to smaller thermal resistances at the hydrophilic surface than those at the hydrophobic surface. Even though the hot wall wettabilities are fixed, Kapitza lengths of the hot wall ($L_{K,h}$) are decreased when the cold wall wettability is strengthened, indicating the coupling interaction among the two solid walls and the liquid film. Here, the cold wall wettabilities are changed by varying β but the hot wall wettability keeps constant. Changing the cold wall wettability alters the liquid temperature profile including the liquid temperature on the hot wall, which is one of the factors to influence the Kapitza length on the hot wall. Thus, changing the cold wall wettability also weakly influences the Kapitza length on the hot wall.

We note that pure heat conduction having a thin liquid film confined in two antisymmetric solid walls was not reported previously, but such a problem with a liquid layer confined in two identical solid walls was studied in Ref. [17], concluding that strong solid-liquid interaction reduces the interfacial thermal resistance but weak interfacial interaction increases the interfacial thermal resistance. The effect of wall wettability on heat transfer has been paid attention [39]. Hydrophilic surface is helpful to enhance heat transfer across the solid-fluid interface [40]. Giri and Hopkins [41] showed that an increase in thermal boundary conductance across strongly bonded solid/liquid interfaces compared to weakly bonded interfaces is due to increased coupling of low-frequency modes when the solid is better wetted by liquid. Local phonon density of states and spectral temperature calculations confirm this

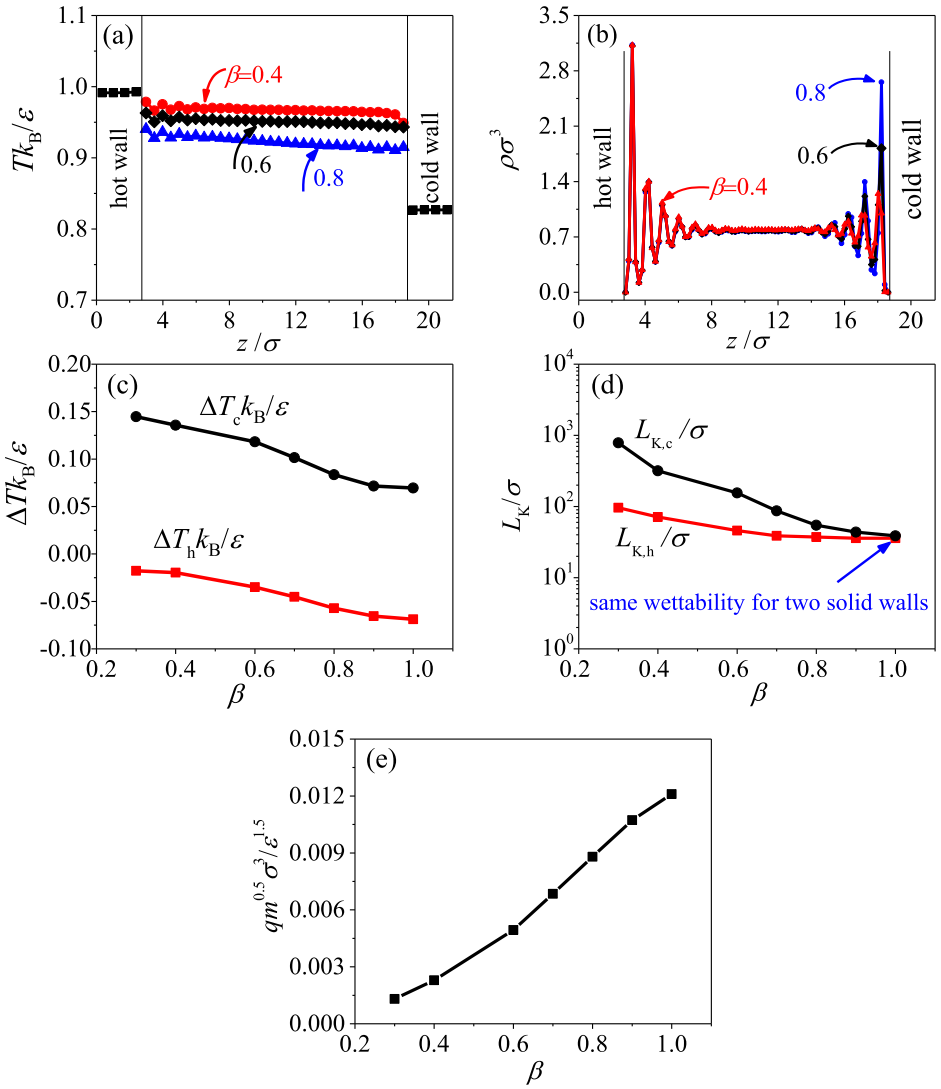

Fig. 3. Effect of cold wall wettability on pure heat conduction in nanochannel (Case study for $F_g^* = 0$, hot wall with $T_h^* = 0.992$, $\alpha = 0.14$, $\beta = 1$, cold wall with $T_c^* = 0.827$, $\alpha = 0.14$, β is changed for different data points. a: temperature profiles; b: density profiles; c: temperature jump at the interface; d: Kapitza length at the interface; e: heat fluxes versus β).

finding. The highly wetted solids couple low frequency phonon energies more efficiently, where the interface of a poorly wetted solid acts like free surfaces. Our asymmetric walls system generally agrees with the relationship between interfacial thermal resistances and surface wettabilities. However, Fig. 3 shows that Kapitza lengths of the hot wall are also influenced by cold wall wettabilities, demonstrating strong coupling and competition of the two solid walls on heat transfer in nanochannel.

4.2. Increased temperature gradient by decreasing hot wall wettability

Fig. 4 shows temperature gradients in the nanochannel can be increased by decreasing hot wall wettabilities. A non-dimensional force of 0.02 is applied to each liquid atom to establish axial velocities. Two cases are considered: one with symmetric walls (both hot and cold walls with $CA = 8.6°$), and the other with asymmetric walls (hydrophobic hot wall with $CA = 115.3°$, and super-hydrophilic cold wall with $CA = 8.6°$). Both slip velocities and temperature jumps are observed on the two solid walls (see Fig. 4a and b). For non-identical wettability system, the velocity profile is non-symmetry. Decrease of hot wall wettability makes liquid atoms traveling faster on the hot wall to elevate bulk velocity in the channel.

The temperature profile in nanochannel is paid attention here. It seems that a linear temperature distribution exists (see Fig. 4b). However, if the profile is examined in a narrow temperature range, it is actually quasi-parabolic (see Fig. 4b). For forced driven nanoflow, liquid temperature at the interface is larger than the wall temperature (positive temperature jump), which is different from pure heat conduction (see Fig. 3). For the latter case, temperature jump is positive on the cold wall but negative on the hot wall. For forced driven nanoflow, positive temperature jump is caused by the viscous heating effect. Under such circumstance, temperature distribution in the nanochannel is not only determined by the hot and cold wall temperatures, but also affected by the viscous heating effect. Two viscous heating mechanisms are involved: heating effect due to friction at the solid-liquid interface, and friction inside the liquid film. The weak interaction between solid and liquid atoms enhances slippages of velocities and temperatures on the walls to elevate temperatures. In other words, the hydrophobic hot wall speeds up the liquid film to yield more external work done on the liquid film, accounting for the elevated liquid temperatures. Here, we note that, by decreasing the

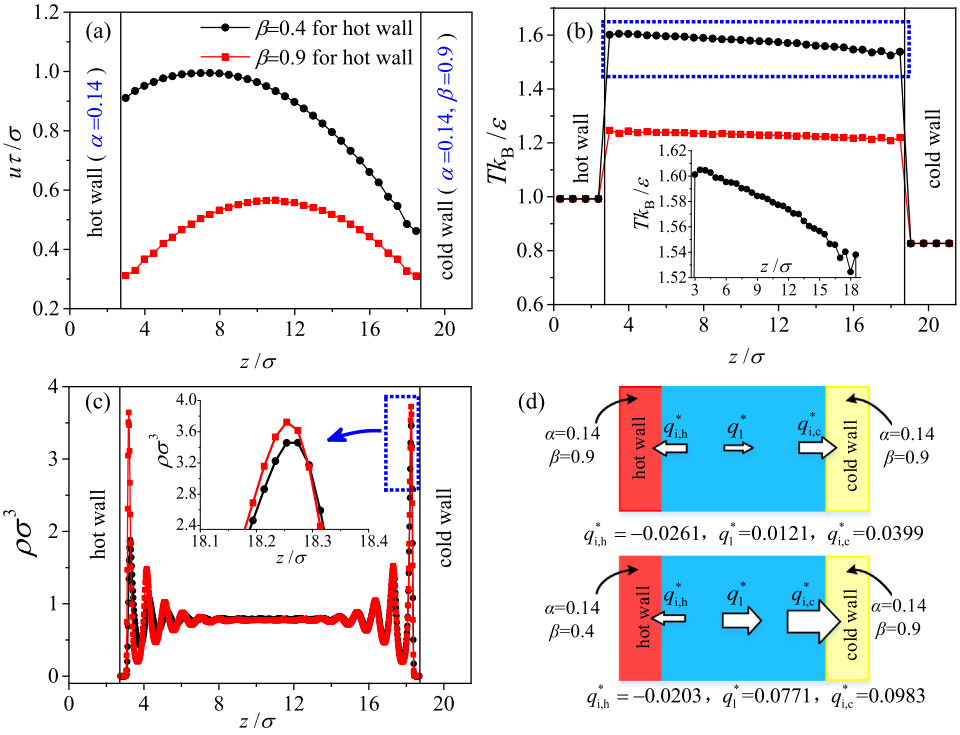

Fig. 4. Effect of hot wall wettability on flow and heat transfer (Case study for $F_g^* = 0.02$, cold wall with $T_c^* = 0.827$, $\alpha = 0.14$, $\beta = 0.9$, hot wall with $T_h^* = 0.992$, $\alpha = 0.14$, β is either 0.4 or 0.9. a: velocity profiles; b: temperature profiles; c: density profiles; d: balance of heat fluxes in nanochannel).

hot wall wettability, the temperature gradient is increased in the nanochannel, which is interest to applications such as biology species separation according to the temperature sensitive nature.

By decreasing the hot wall wettability, not only velocity and temperature on the hot wall, but also velocity and temperature on the cold wall, are increased. Even though the channel height of 16σ is larger than the truncation distance of 3σ, the interfacial effect on the hot wall obviously influences velocity and temperature profiles in bulk liquid region, which also changes velocity and temperature characteristics on the cold wall. The changed slip velocity and temperature jump on the cold wall are caused by the coupling between the two solid walls via the bulk liquid region. Fig. 4c shows that on the hot wall, the peak liquid density at $CA = 8.6°$ with $\beta = 0.9$ is significantly larger than that at $CA = 115.3°$ with $\beta = 0.4$. Even though the cold wall wettability is not changed, the peak liquid density on the cold wall is also influenced by changing the hot wall wettability (see Fig. 4c).

Now, we analyze heat fluxes and heat flow direction. Three heat fluxes are paid attention: heat flux across the hot wall interface ($q_{i,h}$), heat flux in the liquid film (q_l), and heat flux across the cold wall interface ($q_{i,c}$). The asymmetric walls system significantly increases heat flux in the liquid film, due to enhanced friction induced viscous heating on the two solid walls and in the liquid film (see Fig. 4d). In the liquid film, the heat flows from the hot wall side to the cold wall side, called positive heat transfer. On the solid walls, heat flux is influenced by slip velocity on the wall and near wall velocity gradient, the former determines the friction induced heating on the wall, and the latter determines the friction induced heating in the liquid film. By decreasing the hot wall wettability, heat fluxes across the hot wall is not apparently changed by competing the two friction heating effects. The increased slip velocity raises the heating effect on the hot wall, but the decreased velocity gradient near the hot wall side lowers the heating effect to the hot wall. However, for the asymmetric walls system, heat flux across the cold wall is about 2.5 times of that for the identical wall wettability system. The decreased hot wall wettability increases both liquid velocity and velocity gradient near the cold wall, accounting for the raised heat flux across the cold wall.

4.3. Two regimes of heat transfer in the nanochannel

Section 4.2 gave us a clue to modulate temperature gradients in a nano-Janus-interface system. Figs. 5–7 show that negative, zero and positive temperature gradients consecutively occur in the channel height, corresponding to positive heat transfer, no heat transfer and negative heat transfer, respectively. The heat transfer switch can be done by decreasing cold wall wettabilities, applying different forces to liquids, or changing hot wall temperatures. Interfaced by zero heat flux across the two solid walls, positive heat transfer and negative heat transfer appear, which is called the two regimes of heat transfer in this paper. It is noted that in a large channel height, liquid temperatures are always decreased from hot wall side to cold wall side, without slip velocity and temperature jump on solid walls. It is impossible to create negative heat flow sign in a large size channel without the help of interfacial temperature jump.

Fig. 5 shows that the switchable heat transfer is fulfilled by keeping the super-hydrophilic hot wall, while the cold wall wettability is changed from super-hydrophilic ($\beta = 1$ and $CA = 0°$) to hydrophobic ($\beta = 0.4$ and $CA = 115.3°$). All the parameters, including axial velocity u, slip velocity Δu, temperature T, temperature jump ΔT, liquid heat flux q, slip length L_s and Kapitza length L_K are plotted in non-dimensional forms (see Table 1). The subscripts h and c represent hot wall and cold wall, respectively. The pink and gray colors indicate the regimes of positive heat transfer and negative heat transfer, respectively.

In positive heat transfer regime, our numerical simulations start from identical wettabilities of the two solid walls, at which nearly symmetric velocity profile exists in the nanochannel and slip lengths are identical on the two solid walls. However, temperature

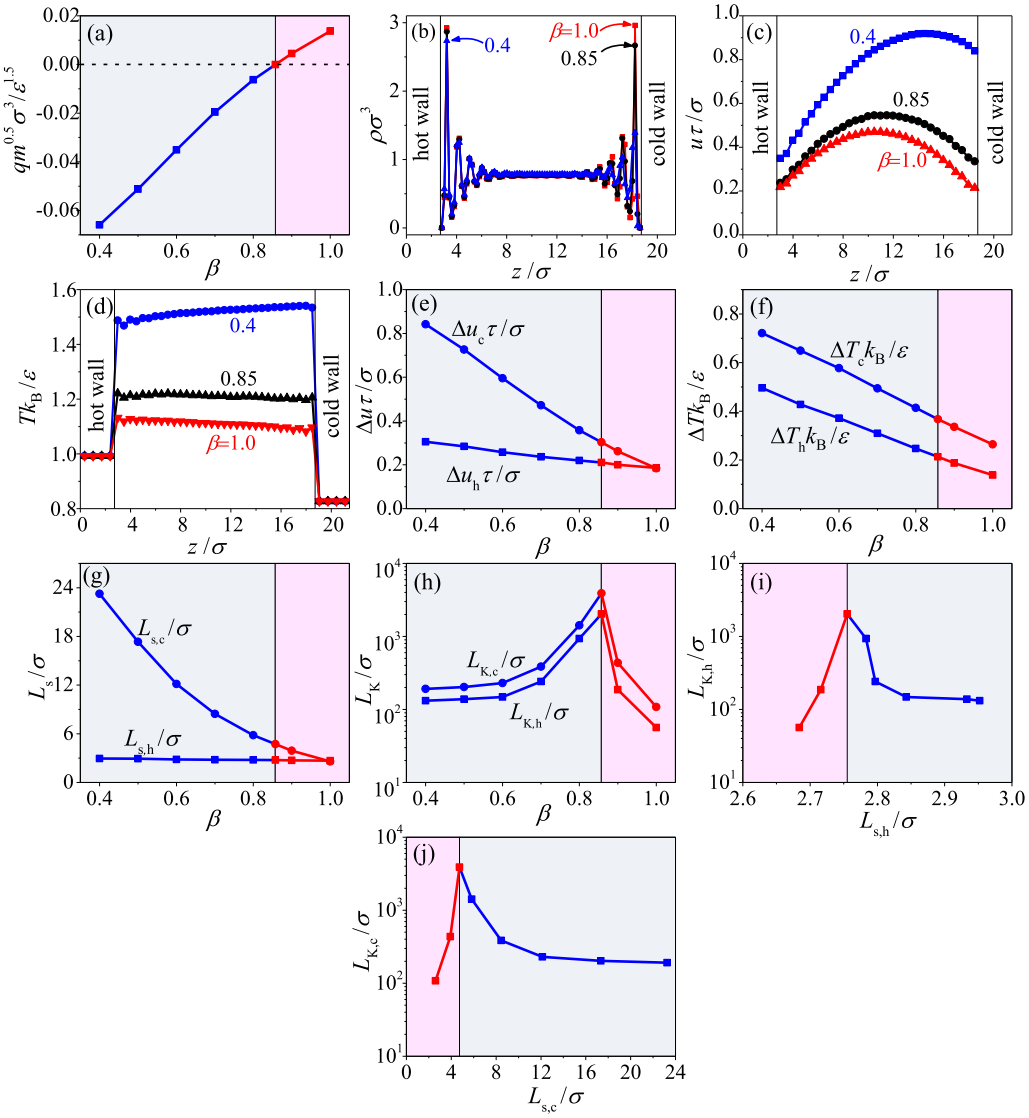

Fig. 5. Effect of cold wall wettability on flow and heat transfer in nanochannel (Case study for $F_g^* = 0.02$, hot wall with $T_h^* = 0.992$, $\alpha = 0.14$, $\beta = 1$, cold wall with $T_c^* = 0.827$, $\alpha = 0.14$, β is changed for different data points. a: heat fluxes versus β; b: density profiles; c: velocity profiles; d: temperature profiles; e: slip velocities versus β; f: temperature jumps versus β; g: slip lengths versus β; h: Kapitza lengths versus β; i and j: relationship of Kapitza length and slip length for hot wall and cold wall, respectively.)

jump on the cold wall is larger than that on the hot wall, indicating that slip velocity is mainly dependent on wall wettabilities, but temperature jump is not only dependent on wall wettabilities, but also dependent on wall temperatures. Both slip velocities and temperature jumps are increased by decreasing β of cold wall. Liquid temperatures on cold wall are increased at a faster speed with decrease of β than those on hot wall, weakening the temperature gradient dT/dz in the channel height direction, until zero temperature gradient occurs at about β =0.85. Negative heat transfer regime takes place beyond the zero temperature gradient. Further decrease of cold wall wettabilities elevates liquid temperature on the cold wall to a level that is larger than that on the hot wall, under which inverse temperature gradient is established.

Over the whole β ranges from 1.0 to 0.4 for the cold wall, both slip velocities and slip lengths of the cold wall are sensitively increased by decreasing β. The increase of solid-liquid interaction leads to a higher peak liquid density near the cold wall. Besides, the weak interaction between cold wall and liquid atoms enhances viscous heating thus elevates liquid temperatures. This effect weakens the liquid density near the hot wall. Since the interaction between liquid and hot wall is stronger, although the slip velocities of hot wall is slightly enhanced, slip lengths on the hot wall are insensitive to the cold wall β values. The situation is changed for temperature jumps, which are increased for both hot and cold walls when the cold wall wettabilities are decreased. Attention is paid to Kapitza lengths, which show very large values near the switch point from pink regime to gray regime. Theoretically, at the switch point, Kapitza length should be infinity due to zero temperature gradient (see Eq. (2)). Both the hot and cold wall share similar trends of Kapitza lengths. It is of interest to explore the relationship between slip lengths L_s and Kapitza lengths L_K. The two solid walls show similar trends of L_K with respect to L_s. In positive heat transfer regime (pink regime), L_K is increased with the increase of L_s, but it is not sensitive to L_s in the negative heat transfer regime (gray regime). Fig. 5a plots non-dimensional heat fluxes inside the liquid film versus cold wall β values. It is observed that the changes of cold wall wettabilities not only switch the heat flow sign, but also modulate the heat flux quantity.

Fig. 6 shows how velocity and temperature distributions are influenced by external forces applied to liquids. The hot wall is

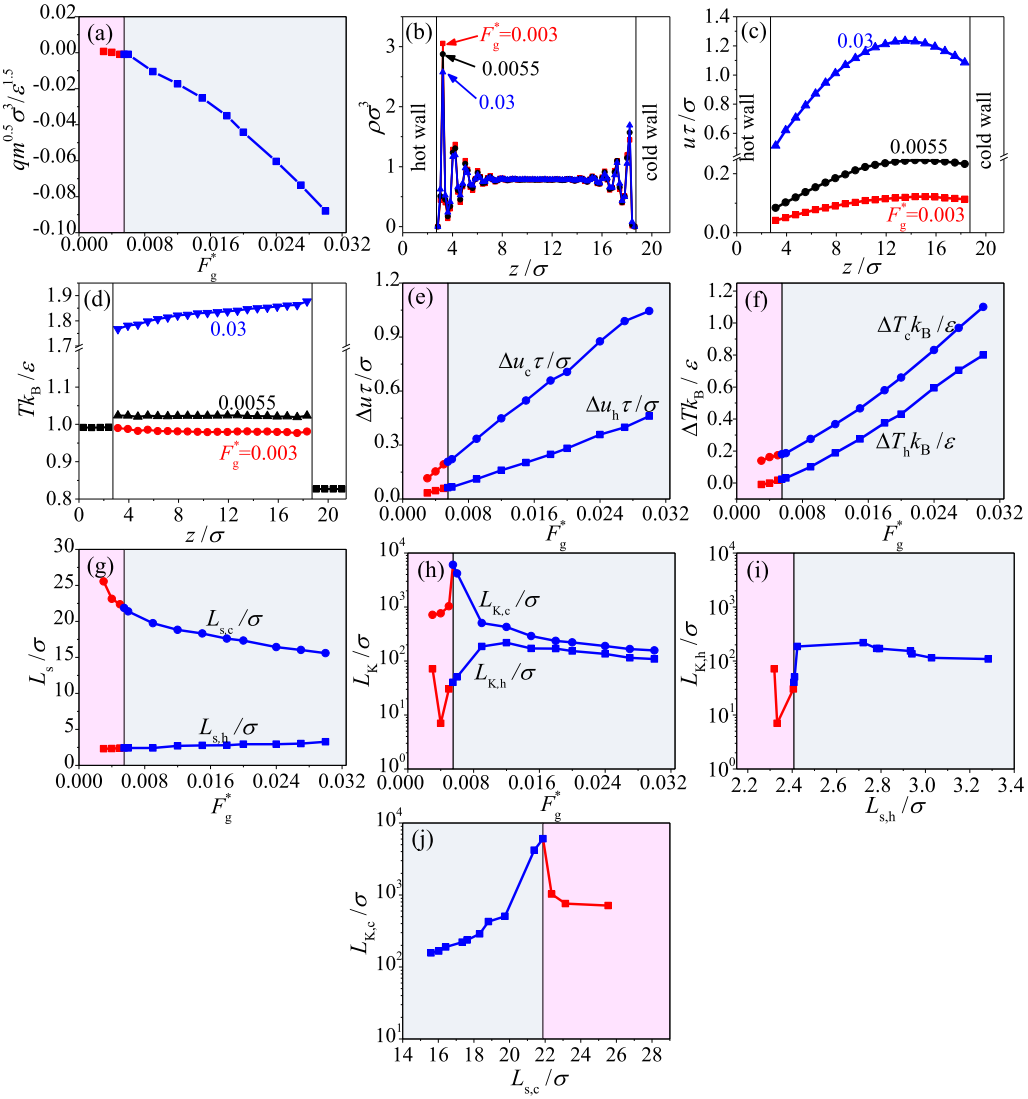

Fig. 6. Effect of non-dimensional force on flow and heat transfer in nanochannel (Case study for hot wall with $T_h^* = 0.992$, $\alpha = 0.14$, $\beta = 1$, cold wall with $T_c^* = 0.827$, $\alpha = 0.14$, $\beta = 0.5$. F_g^* is changed for liquid atoms. a: heat fluxes versus F_g^*; b: density profiles; c: velocity profiles; d: temperature profiles; e: slip velocities versus F_g^*; f: temperature jumps versus F_g^*; g: slip lengths versus F_g^*; h: Kapitza lengths versus F_g^*; i and j: relationship of Kapitza length and slip length for hot wall and cold wall, respectively.)

super-hydrophilic ($CA = 0°$), but the cold wall is with $CA = 91.3°$, which is a transition contact angle from hydrophilicity to hydrophobicity. Due to the weaker interfacial interaction on the cold wall than that on the hot wall, the streaming velocity profile is deformed towards the cold wall side. Slip velocities and temperature jumps are more significant on the cold wall than those on the hot wall. With increases of external forces, the difference of slip velocities on the two solid walls is increased, and temperature jumps are increased for the two solid walls. The sensitive changes of interfacial parameters on the cold wall enlarge negative heat transfer regime but narrows positive heat transfer regime. We note that slip length is determined by interfacial slip velocity divided by velocity gradient on the wall (see Eq. (1)), and Kapitza length is the outcome of interfacial temperature jump divided by temperature gradient on the wall (see Eq. (2)). With increasing of external forces, the movement of liquid atoms is strengthened. Both the hot wall and cold wall show Kapitza lengths independent of external forces, due to identical increase speeds of temperature jumps and temperature gradients on the wall. Fig. 6f and h show the sensitive changes of temperature jumps and temperature gradients (proportion to heat fluxes) by varying external forces.

The two regimes of heat transfer can also be generated in the nanochannel by varying hot wall temperatures (see Fig. 7). The hot wall temperature T_h^* ranges from 0.909 to 2.149. Apparent wettability difference of the two solid walls is used and kept constant. Again, due to the weaker solid-liquid interaction on the cold wall, the axial velocity distribution is non-symmetric but deforms towards the cold wall side. Velocity and temperature slippages are more significant on the cold wall than those on the hot wall. The increasing of hot wall temperature leads to that fluid kinetic energy is up. Thus, fluid atom number near hot wall decreases, which near cold wall conversely increases. Both slip velocities and slip lengths for the two solid walls are less influenced by the varied hot wall temperatures. However, the liquid temperature distribution is sensitively affected by hot wall temperatures. Besides, the change trends of temperature jump with respect to hot wall temperature are thoroughly different for the two solid walls. Higher solid wall temperature increases the kinetic energy of solid atoms, enhancing the energy exchange between solid atoms and liquid atoms. In other words, the increased solid wall temperature ensures free oscillation of liquid atoms, reducing the thermal resistance and Kapitza length on the solid-liquid interface.

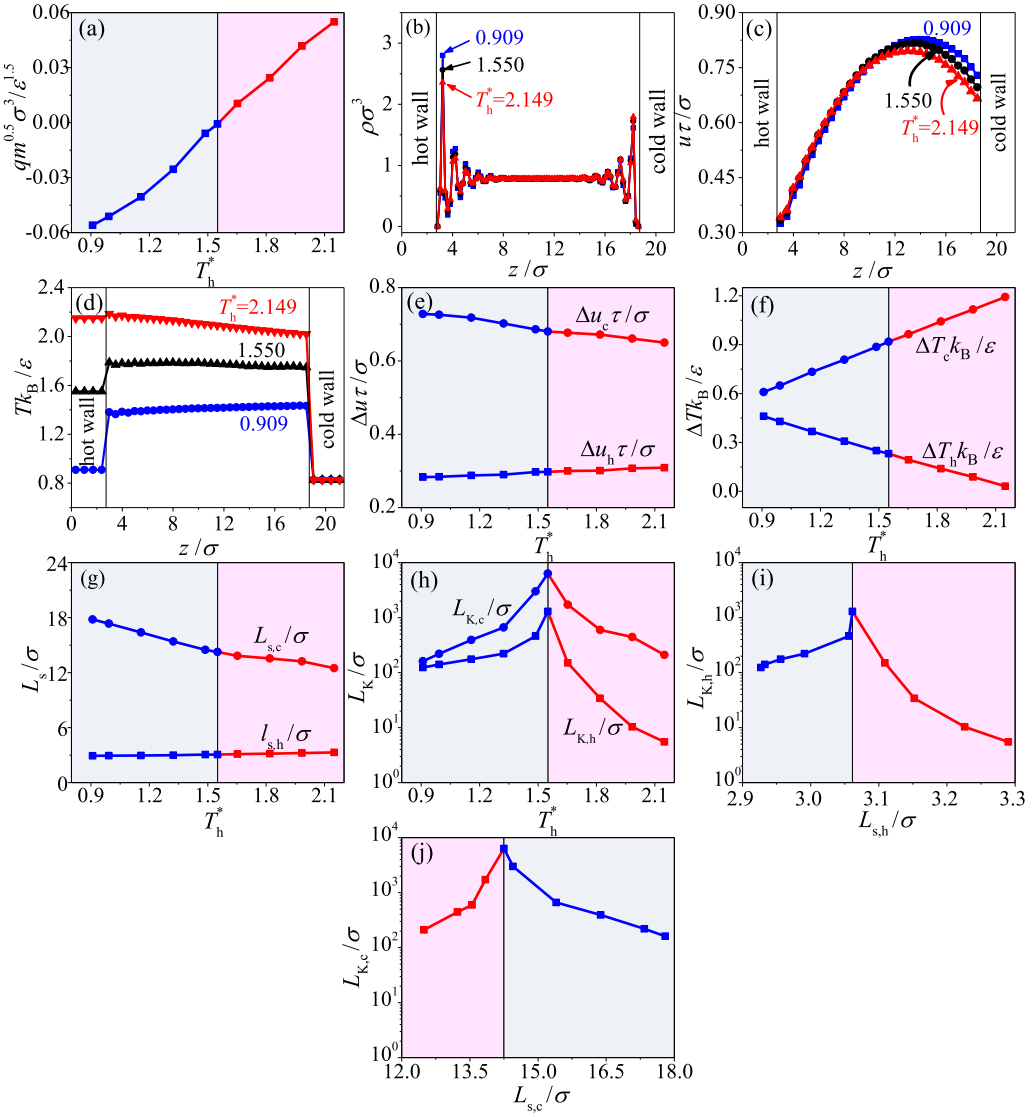

Fig. 7. Effect of hot wall temperatures on flow and heat transfer in nanochannel (Case study for $F_g^* = 0.02$, hot wall with, $\alpha = 0.14$, $\beta = 1$, cold wall with $T_c^* = 0.827$, $\alpha = 0.14$, $\beta = 0.5$. a: heat fluxes versus T_h^*; b: density profiles; c: velocity profiles; d: temperature profiles; e: slip velocities versus T_h^*; f: temperature jumps versus T_h^*; g: slip lengths versus T_h^*; h: Kapitza lengths versus T_h^*; i and j: relationship of Kapitza length and slip length for hot wall and cold wall, respectively.)

For example, the temperature jump at the hot wall is weak at $T_h^* = 2.149$. The elevated hot wall temperatures linearly raise the temperature jumps on the cold wall. The increased hot wall temperature strengthens the thermal oscillation of liquid atoms against their balance locations, evening the liquid density distribution near the hot wall. The relationship between Kapitza lengths and hot wall temperatures or slip lengths show peak phenomenon near the switch point from positive heat transfer to negative heat transfer. Deviating from the peak point, Kapitza lengths are decreased because temperature gradients are increased in both the two directions. The non-dimensional heat fluxes are quasi-linearly changed versus hot wall temperatures. Fig. 7 shows that the balance of liquid temperatures after jumping on the two solid walls can be broken by altering hot wall temperatures to generate switchable heat transfer in the nanochannel.

The force driven flow and heat transfer in identical walls system was investigated in nanoscale in Ref. [42,43]. Either Poiseuille flow or Couette flow were dealt with. When the two solid walls are exactly the same, the velocity profile is symmetry in the nanochannel. The elevated liquid temperatures above the walls are caused by viscous heating, which is dependent on slip velocities on the wall and velocity gradients in liquids. The symmetry viscous heating effect exists in the channel due to the symmetry velocity profile, yielding the same temperature jumps and Kapitza lengths for the two solid walls. In these studies [29–31,42,43], thermal resistances, Kapitza lengths and relationship between velocity and temperature slippages are the same for the two walls.

When different interaction strengths or wettabilities are involved, the problem becomes complicated. Both interfacial flow and thermal parameters are different across the two solid-liquid interfaces. The logic is described as follows. First, non-symmetry velocity profile exists in the channel due to different velocity slips on the two solid walls. Second, the non-symmetry velocity profile causes non-symmetry viscous heating to alter the temperature jumps. Third, liquid temperatures are elevated to different levels on the two solid walls to influence the temperature gradient in the channel.

5. Conclusions

The Non-equilibrium MD simulation is performed for coupled flow and heat transfer in Janus-interface-system. The two solid walls have different wettabilities and temperatures. Contact angles on the two solid walls are given with different solid-liquid interaction strength. Following conclusions are drawn as follows:

1. Pure heat conduction was studied by keeping super-hydrophilic hot wall. Temperature jumps are negative on the hot wall but positive on the cold wall. Kapitza lengths on the two walls are increased with decrease of cold wall wettabilities, indicating strong coupling between the two walls on heat transfer.
2. Decrease of hot wall wettabilities creates more significant velocity and temperature slippages on hot wall than those on cold wall to steepen liquid temperature gradients in nanochannel.
3. Two regimes of heat transfer can be generated, by (1) keeping super-hydrophilic hot wall but changing cold wall wettabilities, (2) keeping super-hydrophilic-hot-wall/hydrophobic-cold-wall but varying external forces applied to liquid, and (3) keeping super-hydrophilic-hot-wall/hydrophobic-cold-wall but varying hot wall temperatures.
4. Heat transfer switch is caused by different temperature jumps on the two walls, and different viscous heating strengths near the cold wall side and hot wall side. The controllable heat transfer is useful for the development of nano-device which needs the temperature sensitive characteristic.

Conflict of interest

The authors declared that there is no conflict of interest.

Acknowledgements

This work was supported by Natural Science Foundation of China (51506026 and 51436004).

Appendix A. Supplementary material

Supplementary data associated with this article can be found, in the online version, at https://doi.org/10.1016/j.ijheatmasstransfer.2018.07.090.

References

[1] M.M. Garimella, S. Koppu, S.S. Kadlaskar, V. Pillutla, Abhijeet, W. Choi, Difference in growth and coalescing patterns of droplets on bi-philic surfaces with varying spatial distribution, J. Colloid Interf. Sci. 505 (2017) 1065–1073.
[2] K. Lum, D. Chandler, J.D. Weeks, Hydrophobicity at small and large length scales, J. Phys. Chem. B 103 (1999) 4570–4577.
[3] J.N. Israelachvili, Intermolecular and Surface Forces, Elsevier, Amsterdam, 2011.
[4] X.Y. Zhang, Y.X. Zhu, S. Granick, Hydrophobicity at a Janus interface, Science 295 (2002) 663–666.
[5] B.J.D. Gans, R. Kita, B. Müller, S. Wiegand, Negative thermodiffusion of polymers and colloids in solvent mixtures, J. Chem. Phys. 118 (2003) 8073–8081.
[6] E. Blums, S. Odenbach, A. Mezulis, M. Maiorov, Soret coefficient of nanoparticles in ferrofluids in the presence of a magnetic field, Phys. Fluids 10 (1998) 2155–2163.
[7] G.E.H. Mohamed, The fluid mechanics of microdevices-the freeman scholar lecture, J. Fliuds Eng. 121 (1999) 5–33.
[8] C. Bakli, S. Chakraborty, Slippery to sticky transition of hydrophobic nanochannels, Nano Lett. 2015 (15) (2015) 7497–7502.
[9] G. Nagayama, P. Cheng, Effects of interface wettability on microscale flow by molecular dynamics simulation, Int. J. Heat Mass Transf. 47 (2004) 501–513.
[10] J.L. Xu, Z.Q. Zhou, X.D. Xu, Molecular dynamics simulation of micro-poiseuille flow for liquid argon in nanoscale, Int. J. Numer. Methods Heat Fluid Flow 14 (2004) 664–688.
[11] J.L. Xu, Y. Li, Boundary conditions at the solid–liquid surface over the multiscale channel size from nanometer to micron, Int. J. Heat Mass Transf. 50 (2007) 2571–2581.
[12] U. Ulmanella, C.M. Ho, Molecular effects on boundary condition in micronanoliquid flows, Phys. Fluids 20 (2008) 201512.
[13] J. Ghorbanian, A. Beskok, Scale effects in nano-channel liquid flows, Microfluid Nanofluid 20 (2016) 121.
[14] T.Q. Vo, B.H. Kim, Transport phenomena of water in molecular fluidic channels, Sci. Rep. 6 (2016) 33881.
[15] W.A. Little, Can, The transport of heat between dissimilar solids at low temperatures, J. Phys. 37 (1996) 334–349.
[16] R.S. Prasher, P.E. Phelan, A scattering-mediated acoustic mismatch model for the prediction of thermal boundary resistance, J. Heat Transf. 123 (2001) 105–112.
[17] L. Xue, P. Keblinski, S.R. Phillpot, S.U.S. Choi, J.A. Eastman, Two regimes of thermal resistance at a liquid–solid interface, J. Chem. Phys. 118 (2003) 337–339.
[18] P.A. Thompson, S.M. Troian, A general boundary condition for liquid flow at solid surfaces, Nature 389 (1997) 360–362.
[19] L. Bao, N.V. Priezjev, H. Hu, K. Luo, Effects of viscous heating and wall-fluid interaction energy on rate-dependent slip behavior of simple fluids, Phys. Rev. E 96 (2017) 033110.
[20] T.Q. Vo, B.H. Kim, Interface thermal resistance between liquid water and various metallic surfaces, Int. J. Precis. Eng. Manuf. 16 (2015) 1341–1346.
[21] C.Y. Soong, T.H. Yen, P.Y. Tzeng, Molecular dynamics simulation of nanochannel flows with effects of wall lattice-fluid interactions, Phys. Rev. E 76 (2007) 036303.
[22] B.Y. Cao, M. Chen, Z.Y. Guo, Liquid flow in surface-nanostructured channels studied by molecular dynamics simulation, Phys. Rev. E 74 (2006) 066311.
[23] J. Servantie, M. Müller, Temperature dependence of the slip length in polymer melts at attractive surfaces, Phys. Rev. Lett. 101 (2008) 026101.
[24] V. Bitrián, J. Principe, Driving mechanisms and streamwise homogeneity in molecular dynamics simulations of nanochannel flows, Phys. Rev. Fluid 3 (2018) 014202.
[25] J. Ghorbanian, A.T. Celebi, A. Beskok, A phenomenological continuum model for force-driven nano-channel liquid flows, J. Chem. Phys. 145 (2016) 184109.
[26] N.V. Priezjev, Rate-dependent slip boundary conditions for simple fluids, Phys. Rev. E 75 (2007) 051605.
[27] J. Ghorbanian, A. Beskok, Temperature profiles and heat fluxes observed in molecular dynamics simulations of force-driven liquid flows, J. Chem. Phys. 19 (2017) 10317–10325.
[28] Q.W. Chen, L.Y. Meng, Q.K. Li, D. Wang, W. Guo, Z.G. Shuai, Water transport and purification in nanochannels controlled by asymmetric wettability, Small 7 (2011) 2225–2231.
[29] F. Faraji, A. Rajabpour, Fluid heating in a nano-scale poiseuille flow: a non-equilibrium molecular dynamics study, Curr. Appl. Phys. 17 (2017) 1646–1654.
[30] C. Liu, H.B. Fan, K. Zhang, M.F. Matthew, Z.G. Li, Flow dependence of interfacial thermal resistance in nanochannels, J. Chem. Phys. 132 (2010) 094703.
[31] D.C. Marable, S. Shin, A.Y. Nobakht, Investigation into the microscopic mechanisms influencing convective heat transfer of water flow in graphene nanochannels, Int. J. Heat Mass Transf. 109 (2017) 28–39.
[32] A. Pham, M. Barisik, B.H. Kim, Pressure dependence of Kapitza resistance at gold/water and silicon/water interfaces, J. Chem. Phys. 139 (2013) 244702.
[33] Y. Feng, X. Liang, Heat transfer characteristics in an asymmetrical solid–liquid system by molecular dynamics simulations, Int. J. Thermophys. 36 (2015) 1519–1529.
[34] Y. Pan, D. Poulikakos, J. Walther, G. Yadigaroglu, Molecular dynamics simulation of vaporization of an ultra-thin liquid argon layer on a surface, Int. J. Heat Mass Transf. 45 (2002) 2087–2100.
[35] J. Delhommelle, P. Millié, Inadequacy of the Lorentz-Berthelot combining rules for accurate predictions of equilibrium properties by molecular simulation, Mol. Phys. 99 (2001) 619–625.
[36] J. Vera, Y. Bayazitoglu, Temperature and heat flux dependence of thermal resistance of water/metal nanoparticle interfaces at sub-boiling temperatures, Int. J. Heat Mass Transf. 86 (2015) 433–442.
[37] D. Torii, T. Ohara, Molecular dynamics study on ultrathin liquid water film sheared between platinum solid walls: liquid structure and energy and momentum transfer, J. Chem. Phys. 126 (2007) 154706.
[38] G. Nagayama, M. Kawagoe, A. Tokunaga, T. Tsuruta, On the evaporation rate of ultra-thin liquid film at the nanostructured surface: a molecular dynamics study, Int. J. Therm. Sci. 49 (2010) 59–66.
[39] M. Barisik, A. Beskok, Temperature dependence of thermal resistance at the water/silicon interface, Int. J. Therm. Sci. 77 (2014) 47–54.
[40] X. Wang, P. Cheng, X. Quan, Molecular dynamics simulations of thermal boundary resistances in a liquid between two solid walls separated by a nano gap, Int. Commun Heat Mass. 77 (2016) 183–189.
[41] A. Giri, P.E. Hopkins, Spectral analysis of thermal boundary conductance across solid/classical liquid interfaces: a molecular dynamics study, Appl. Phys. Lett. 105 (2014) 033106.
[42] J. Sun, W. Wang, H.S. Wang, Viscous dissipation effect in nano-confined shear flows: a comparative study between molecular dynamics and multi-scale hybrid simulations, Microfluid Nanofluid 18 (2015) 103–109.
[43] Z. Li, Surface effects on friction-induced fluid heating in nanochannel flows, Phys. Rev. E 79 (2009) 026312.